Proceedings of the ASME 2013 Dynamic Systems and Control Conference
DSCC2013
October 21-23, 2013, Palo Alto, California, USA

DSCC2013-3883

SNAKEBOARD MOTION PLANNING WITH LOCAL TRAJECTORY INFORMATION

Tony Dear
Robotics Institute
Carnegie Mellon University
Pittsburgh, Pennsylvania 15232
tonydear@cmu.edu

Ross L. Hatton
School of Mechanical, Industrial,
and Manufacturing Engineering
Oregon State University
Corvallis, Oregon 97331
ross.hatton@oregonstate.edu

Matthew Travers
Howie Choset
Robotics Institute
Carnegie Mellon University
Pittsburgh, Pennsylvania 15232
mtravers@andrew.cmu.edu,
choset@cs.cmu.edu

ABSTRACT

We address trajectory generation for the snakeboard, a system commonly studied in the geometric mechanics community. Our approach derives a solution using body coordinates and local trajectory information, leading to a more intuitive solution compared to prior work. The simple forms of the solution clearly show how they depend on local curvature and desired velocity profile, allowing for a description of some simple motion primitives. We readily propose techniques to navigate paths, including those with sharp corners, by taking advantage of the snakeboard's singular configuration, as well as discuss some implications of torque limits.

1 INTRODUCTION

The snakeboard is a canonical example of a mixed nonholonomic mechanical system, one whose motion is governed by both kinematic constraints and dynamics [1, 2]. The snakeboard shown in Fig. 1 consists of two sets of wheels that can rotate about the center point of the axle. To ride the snakeboard, one alternates between rotating one's torso with one's ankles to move the wheelsets. The mechanical model in Fig. 2 has a rotor situated at the center of the longitudinal axis to simulate the human rider's torso. The rotor and wheel angles are actuated, and the latter act as constraints, allowing the snakeboard to locomote when its joint angles are changing.

Early approaches in snakeboard analysis employed extensive use of gaits, or cyclic changes in the joint inputs. A key feature of using gaits for locomotion is that they allow for a system to progress along a trajectory despite joint limits. Ostrowski et al. [3] used techniques developed by Murray and Sastry [4] to evaluate sinusoidal steering controllers to move the snakeboard in various basis directions. Ostrowski et al. [5] then extended this approach by using optimal control to select optimal gaits for their controllers.

Figure 1. A SNAKEBOARD COMPOSED OF A RIGID AXIS AND TWO FOOTRESTS ON ROTATING WHEELSETS.

Bullo and Lewis [6] addressed the motion planning problem of taking a snakeboard to a desired goal state from a given start state by using vector field analysis techniques developed by Bullo et al. [7]. In these solutions, the snakeboard's overall trajectory was actually a concatenation of separate kinematic trajectory segments between the start and goal states.

In order to study the contributions of gaits to locomotion, Shammas et al. [2] analyzed gait motions as a combination of geometric and dynamic displacement contributions. They were able to propose gaits that contribute to motion along a desired direction, although their method did not address the full motion planning problem of finding a trajectory between two states.

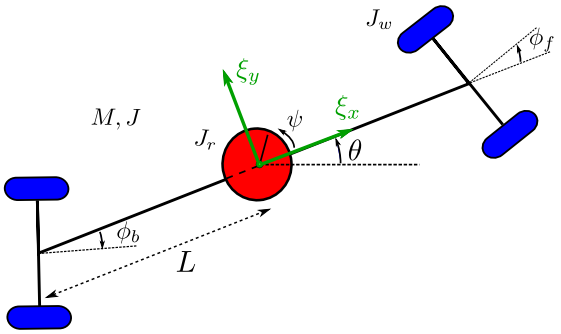

Figure 2. THE CONFIGURATION OF THE SNAKEBOARD.

More recently, Shammas and de Oliveira [8, 9] developed a solution for the snakeboard in which the problem specification is an entire trajectory, not just the endpoint configurations. Their approach assumes that the joint motions are unconstrained and thus do not require gaits, in contrast to previous work. Without the restriction of gaits, they are able to analytically solve for the joint angles in order to follow the prescribed trajectory.

In this paper, we build upon the results of [8, 9] and propose a simpler representation of the solution using only body coordinates and local curvature information of the desired path. We have found that this approach yields much insight into the properties and limits of the control problem. This solution also presents us with simple primitives that can be stitched together to form more complex trajectories. Finally, we comment on some types of the paths that the snakeboard can or cannot follow and show some simulation results of the derived solutions.

2 EQUATIONS OF MOTION

The snakeboard's configuration, shown in Fig. 2, is given by $q \in Q = (g, r)$, where the position variables $g = (x, y, \theta) \in G = SE(2)$ locate the snakeboard in the world and the shape variables $r = (\psi, \phi) \in M = \mathbb{S}^1 \times \mathbb{S}^1$ describe the system's joint configurations.[1] The variables x and y denote the global position of the snakeboard's center of mass, while θ denotes the system's longitudinal axis orientation with respect to the horizontal. ψ denotes the rotor angle, and ϕ_f and ϕ_b denote the angles of the front and back sets of wheels, respectively, both with respect to the longitudinal axis. We enforce the constraint $\phi_f = -\phi_b$ and henceforth use $\phi = \phi_f$, which will simplify the problem while still allowing for a full solution.

The world velocity of the system is $\dot{g} = (\dot{x}, \dot{y}, \dot{\theta})$. However, in this paper, we work with the body velocities ξ instead, which has components in the forward, lateral, and rotation directions. They are related to the world velocities by the following mapping[2].

$$\xi = \begin{pmatrix} \xi_x \\ \xi_y \\ \xi_\theta \end{pmatrix} = \begin{pmatrix} \cos\theta & \sin\theta & 0 \\ -\sin\theta & \cos\theta & 0 \\ 0 & 0 & 1 \end{pmatrix} \begin{pmatrix} \dot{x} \\ \dot{y} \\ \dot{\theta} \end{pmatrix} \tag{1}$$

The snakeboard's mass and inertia are denoted M and J, while the rotor and wheel inertias are denoted J_r, and J_w, respectively. We will assume as in [9] that $ML^2 = J + J_r + 2J_w$ is the total inertia of the system, where the total length of the snakeboard is $2L$.

The snakeboard's Lagrangian, which is simply its kinetic energy, is invariant to changes in the system's position or orientation in space, so we can express it in body velocities instead of world velocities. In the absence of constraints, this property is equivalent to an inherent *symmetry* of the system; the fact that the dynamics are unchanged with respect to rigid transformations of the body frame corresponds to momentum conservation. The Lagrangian in the body frame is

$$l(\xi, \dot{r}) = \frac{M(\xi_x^2 + \xi_y^2 + L^2\xi_\theta^2) + J_r(2\xi_\theta\dot{\psi} + \dot{\psi}^2) + 2J_w\dot{\phi}^2}{2}. \tag{2}$$

The no slip conditions on the wheels give rise to the system's nonholonomic constraints. Like the Lagrangian, the constraints are invariant with respect to transformations in $SE(2)$, so they can be written in terms of the local body coordinates only. They can be expressed in *Pfaffian form* $\omega(r)\xi = 0$, where

$$\omega(r) = \begin{pmatrix} -\sin\phi & \cos\phi & L\cos\phi \\ \sin\phi & \cos\phi & -L\cos\phi \end{pmatrix}. \tag{3}$$

Given the Lagrangian and constraints, it is possible to completely determine the evolution of the system through the Euler-Lagrange equations of motion, *i.e.*,

$$\begin{aligned} \frac{d}{dt}\left(\frac{\partial l(\xi,\dot{r})}{\partial \xi_i}\right) + \sum_{j=1}^{2} \lambda_j \omega_i^j(r) = 0, \quad i = 1,2,3 \\ \frac{d}{dt}\left(\frac{\partial l(\xi,\dot{r})}{\partial \dot{\psi}}\right) = \tau_\psi, \quad \frac{d}{dt}\left(\frac{\partial l(\xi,\dot{r})}{\partial \dot{\phi}}\right) = \tau_\phi. \end{aligned} \tag{4}$$

Here, i indexes the body coordinate, the Lagrange multiplier for the jth constraint is λ_j, and the input torques for the rotor and wheel sets are τ_ψ and τ_ϕ, respectively.

[1] In the context of geometric mechanics, $Q = M \times G$ is a *trivial principal fiber bundle*, M is the *base space*, and G is the *fiber space*.

[2] $G = SE(2)$ is a *Lie group*, whose tangent space is equipped with the *lifted left action* corresponding to the mapping above. The body velocity ξ lives in the *Lie algebra* $\mathfrak{g}$, which is homeomorphic to the tangent space at the identity of the group. For further reading on the topic, see [10] and [11].

However, the Euler-Lagrange equations do not allow an easy solution for the inverse motion planning problem. Given a planned trajectory, it is difficult to invert the equations of motion to derive the input forces and torques required to follow it. Similar to previous work, the approach in this paper uses tools from geometric mechanics for an alternate formulation of the problem.

From Eq. (2) and Eq. (3) we first compute the *nonholonomic momentum* [12] using the definition $p = \frac{\partial l}{\partial \xi}\Omega^T$, where Ω^T is a basis of the null space of ω. The nonholonomic momentum thus projects the *generalized momentum* $\frac{\partial l}{\partial \xi}$ onto a basis that respects the constraints. We choose $\Omega = \big(L,\, 0,\, \tan\phi\big)$ and find

$$p = ML(\xi_x + L\xi_\theta \tan\phi) + J_r\dot{\psi}\tan\phi. \tag{5}$$

Next we examine how joint velocities and and momentum determine resultant body velocities. Combining the constraints Eq. (3) and the momentum definition Eq. (5), we find the following system of equations:[3]

$$\xi = -\begin{pmatrix} \frac{J_r \sin 2\phi}{2ML} & 0 \\ 0 & 0 \\ \frac{J_r \sin^2\phi}{ML^2} & 0 \end{pmatrix} \begin{pmatrix} \dot{\psi} \\ \dot{\phi} \end{pmatrix} + \begin{pmatrix} \frac{\cos^2\phi}{ML} \\ 0 \\ \frac{\sin 2\phi}{2ML^2} \end{pmatrix} p. \tag{6}$$

Finally, we solve for the momentum evolution equation [12], which describes how the momentum changes in time. This can be derived by substituting Eq. (6) into the Euler-Lagrange equations of motion Eq. (4) for the body velocities. One can then eliminate the Lagrange multipliers and solve for $\dot{p}$ to obtain

$$\dot{p} = \dot{\phi}(p\tan\phi + J_r\dot{\psi}). \tag{7}$$

3 THE MOTION PLANNING PROBLEM

The motion planning problem for the snakeboard is to take a specified path between a start and a goal location in space, and determine a trajectory for the rotor and wheel angles that propels the snakeboard along the path. The path to be followed is a curve in space, which can be defined by its curvature as a function of its arclength, along with initial conditions. Since the snakeboard is moving along the curve in time, we also dictate the amount of distance to be traveled as a function of time.

We formulate the problem as follows. The spatial curve to be followed will be parameterized in s and defined in terms of curvature. We define $\kappa(s)$ and $r(t)$ to be the curvature and desired distance functions, respectively, where

$$\kappa : \mathbb{R} \to \mathbb{R}, \tag{8}$$

$$r : [0, T] \to \mathbb{R}. \tag{9}$$

[3]This is the *reconstruction equation*, which has the form $\xi = -A(r)\dot{r} + \Gamma(r)p$.

The curvature $\kappa(s)$ is positive if the unit tangent vector along the curve rotates in a counter-clockwise direction as a function of arclength; otherwise, it is negative. We assume that we are given initial conditions that describe the starting location on the curve.

The distance $r(t)$ tells us how much distance to travel over time. Note that it is possible to go backward if $\dot{r} < 0$. Since the arclength is equivalent to distance traveled, we have $s = r(t)$. In general, we also require that r be twice-differentiable and κ be once-differentiable. Then the function

$$c(t) := \kappa(s) = \kappa(r(t)) \tag{10}$$

is a differentiable path curvature function parameterized in time.

We wish to solve for the shape trajectory $\phi(t)$ and shape velocity $\dot{\psi}(t)$ such that the x-axis of the local body frame is tangent to the curve described by $c(t)$, and the total distance traveled along the curve by the snakeboard's center of mass is equal to $r(t)$. Note that we do not have to solve for $\psi(t)$ explicitly, since it does not appear in any of the equations of motion. Physically, the orientation of the rotor does not matter due to rotational symmetry; only changes in its velocity contribute to the overall system dynamics.

This method of path parameterization is different from that of [9], where the path is paramerized using world coordinates, namely x and y. Although that approach explicitly provides the center of mass location at any given time, it forces the adoption of a fixed inertial frame. This in turn significantly increases the complexity of the solution with the use of intermediary variables.

4 THE SNAKEBOARD SOLUTION

Given the problem specification, we can now explicitly solve for the joint angles that will allow the snakeboard to adhere to the desired curvature and arclength functions. We follow a procedure similar to that of [9], but the resultant solution is much simpler.

4.1 The Joint Angles

We first obtain a solution for the wheel angles $\phi(t)$ by examining the geometry of the snakeboard on the trajectory at any given point in time (Fig. 3). We have that the longitudinal axis is instantaneously tangent to the path at the point P. Then the snakeboard's longitudinal axis must be orthogonal to the curvature radius R, which is simply the inverse of the curvature itself.

By trigonometry, the angle between the front wheels' axis and the radius of curvature is equal to ϕ. Thus, the wheel angles and the snakeboard's steering profile are completely determined by the local curvature of the path to be followed:

$$\phi(t) = \phi_f(t) = \tan^{-1}(Lc(t)) = -\phi_b(t). \tag{11}$$

The tangency requirement also requires that the snakeboard's forward velocity be equal to the rate of change in arclength, $\dot{r}(t)$. Since $r(t)$ and thus $\dot{r}(t)$ are provided, we can solve the remainder of the problem assuming that ξ_x is known:

$$\xi_x(t) = \dot{r}(t). \tag{12}$$

We can also solve for the y and θ components of the body velocity. They are completely specified by the constraints Eq. (3), since we now know the wheel angles $\phi(t)$:

$$\xi_y(t) = 0, \tag{13}$$

$$\xi_\theta(t) = \frac{\tan\phi(t)}{L}\xi_x(t) = c(t)\dot{r}(t). \tag{14}$$

The other shape input to be determined is the rotor velocity, which controls the forward velocity of the snakeboard. We differentiate the momentum Eq. (5) to obtain an expression for $\dot{p}$. This can then be equated to the momentum evolution Eq. (7):

$$\begin{aligned}\dot{p} &= ML(\dot{\xi}_x + L\dot{\xi}_\theta\tan\phi + L\xi_\theta\dot{\phi}\sec^2\phi) + J_r(\dot{\psi}\dot{\phi}\sec^2\phi + \ddot{\psi}\tan\phi)\\ &= ML\dot{\phi}(\xi_x\tan\phi + L\xi_\theta\tan^2\phi) + J_r\dot{\phi}(\dot{\psi}\tan^2\phi + \dot{\psi}).\end{aligned} \tag{15}$$

By substituting the expression for ξ_θ from Eq. (14) into Eq. (15), we can obtain a second-order differential equation for ψ, which is solvable in the known quantities.

$$J_r\ddot{\psi} = -\frac{2ML}{\sin 2\phi}\dot{\xi}_x - ML\dot{\phi}\sec^2\phi\xi_x \tag{16}$$

If we integrate this equation once, we obtain a solution for $\dot{\psi}$ as a definite integral of the path parameterization functions:

$$\dot{\psi}(t) = -\frac{M}{J_r}\int_0^t \frac{1+L^2c(\tau)^2}{c(\tau)}\ddot{r}(\tau)\,d\tau - \frac{ML^2}{J_r}\int_0^t \dot{c}(\tau)\dot{r}(\tau)\,d\tau. \tag{17}$$

4.2 Special Cases

From the solutions to the shape variables of the snakeboard, some simple primitives governing its motion can be inferred for special cases of curvature and forward speed. We will also discuss a method for dealing with non-differentiable paths, for which Eq. (17) does not have a solution. This case was not addressed by the solution of [9].

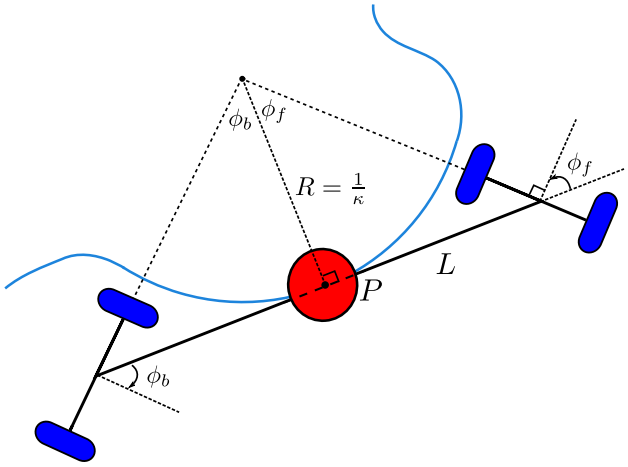

Figure 3. THE GEOMETRY OF THE SNAKEBOARD'S TRAJECTORY.

4.2.1 Constant Forward Velocity. For constant forward velocity, arclength is increasing at a constant rate; $\dot{r}$ is constant and $\ddot{r} = 0$. If t_0 is the time at which the velocity becomes constant, then the rotor velocity has the following solution:

$$\dot{\psi}(t) = -\frac{ML^2}{J_r}\Big(c(t) - c(t_0)\Big)\dot{r} + \dot{\psi}(t_0). \tag{18}$$

For a general trajectory in which the goal is to simply maintain a constant forward velocity, the change in rotor velocity thus varies linearly with the curvature of the path to be followed.

4.2.2 Zero Curvature. When the curvature $\kappa = 0$, the path becomes straight, and both the front and back sets of wheels are aligned with the path, *i.e.*,

$$\phi(t) = 0. \tag{19}$$

In this configuration, $\xi_y = \xi_\theta = 0$, but there is no prescription for ξ_x. This results in a symmetry in the longitudinal direction, which corresponds to the conservation of linear momentum. The snakeboard must enter and leave this regime with the same momentum, implying that the forward velocity remains constant.

Because of the invariance in forward velocity, the rotor has no effect on the motion of the snakeboard, and so its orientation and velocity can be reset arbitrarily during the period in which the curvature remains 0. This can be a useful technique for preventing the rotor's velocity from becoming too large.

4.2.3 Constant, Nonzero Curvature. For constant, nonzero curvature $c = c_0$, Eq. (11) again yields a constant wheel

angle solution:

$$\phi(t) = \phi_0 = \tan^{-1}(Lc_0). \tag{20}$$

Thus $\dot{\phi} = 0$, and from Eq. (7) we can also conclude that $\dot{p} = 0$. The total momentum must be conserved such that $p = p_0$ during the interval on which the snakeboard moves along the constant curvature section, where p_0 is the momentum built up by the system at the time that it enters this section.

If t_0 is the time at which the curvature becomes constant, then the rotor velocity profile is given as follows:

$$\dot{\psi}(t) = -\frac{M}{J_r}\left(\frac{1+L^2c_0^2}{c_0}\right)(\dot{r}(t) - \dot{r}(t_0)) + \dot{\psi}(t_0). \tag{21}$$

The rotor velocity varies linearly with the desired forward velocity for a constant curvature path. This is analogous to Eq. (18), the case of constant forward velocity and changing curvature.

4.2.4 The Singular Configuration. When the path curvature goes to infinity, as at a sharp corner, the path becomes non-differentiable. The solution for the wheel angles is

$$\phi(t) = \pm\frac{\pi}{2}. \tag{22}$$

The wheels are oriented at right angles to the snakeboard's axis, and so the system can only turn in place while being unable to move forward. Our previous stipulations for the body velocities are invalid for this singular configuration, as we now have that $\xi_x = 0$ and Eq. (14) no longer holds.

However, we can relate the rotor angular velocity to that of the snakeboard. Substituting $\phi(t) = \pm\frac{\pi}{2}$ into Eq. (6) gives us

$$\xi_\theta = -\frac{J_r}{ML^2}\dot{\psi}(t) + \dot{\psi}(t_0), \tag{23}$$

where t_0 is the time at which the snakeboard achieves the singular configuration. This is simply a statement of the conservation of angular momentum about the snakeboard's center of rotation, where the momentum comes from the rotor velocity at t_0.

As shown in Fig. 4, infinite curvature can occur discontinuously at a sharp corner in the path. At this location, c is instantaneously characterized by an impulse function, and we cannot use Eq. (17) to solve for the inverse kinematics of the joint angles. Physically, an infinite amount of force is required to instantaneously change the wheel angles in a discontinuous manner if the snakeboard's forward velocity is nonzero.

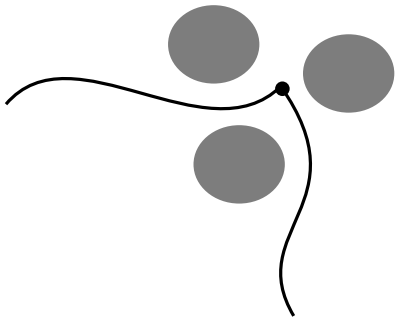

Figure 4. AVOIDING SOME OBSTACLES VIA A SHARP CORNER.

Since corners may appear in a physical trajectory, we propose the following technique to traverse them. The snakeboard must be at rest before and after turning the corner, so we require that a corner occurs at the intersection of two curves with nonzero curvature. Thus, the forward velocity $\dot{r}$ must encode the corner with zero forward velocity.

The snakeboard first steers into the corner by following the path curvature and then stops completely by spinning the rotor according to Eq. (17). Next the wheel angles will turn to achieve $\phi = \frac{\pi}{2}$. From Eq. (23), we can use the rotor to make the snakeboard spin in place until its axis is tangent to the new path segment. In the last step, we rotate the wheel axes to match the new curvature and resume rotor movement to continue moving again.

The described maneuver is equivalent to restarting the snakeboard from a resting configuration. The initial condition of the new segment's orientation is encoded in the magnitude of the impulse function, which measures the change in orientation between the two path segments.

4.3 Allowed and Prohibited Trajectories

We now consider the effect of torque limits on the snakeboard's ability to handle trajectories, as our solution assumes that joint angles can accelerate arbitrarily quickly, which may be nonphysical. We emphasize that we can easily interpret the physical meanings of such limits due to the simple forms of our solutions.

Limits on the wheel torques τ_ϕ will limit how fast the snakeboard can change direction. If the wheels' maximum acceleration is $\ddot{\phi}_m$, then from the second derivative of Eq. (11) the curvature function c must satisfy

$$\left|\frac{1}{1+\tilde{c}^2}\left(\ddot{\tilde{c}} - \frac{2\tilde{c}\dot{\tilde{c}}^2}{1+\tilde{c}^2}\right)\right| \leq \ddot{\phi}_m, \tag{24}$$

where we define the scaled curvature $\tilde{c} = Lc$. If this inequality does not hold, then the snakeboard will be unable to adhere to the prescribed path cuvature.

We can interpret Eq. (24) as a limit on the sharpness of turns that the snakeboard can make. An example curvature characteristic of a sharp turn is shown in Fig. 5, along with its derivatives. Notice that the zero of $\dot{\tilde{c}}$ coincides with an extremum of $\ddot{\tilde{c}}$, while the extrema of $\dot{\tilde{c}}$ coincide with the zeros of $\ddot{\tilde{c}}$.

At these points, the left-hand side of Eq. (24) becomes large, and the magnitudes of $\dot{\tilde{c}}$ and $\ddot{\tilde{c}}$ scale with the sharpness of the turn. In the limit as $c \to \infty$ and tends toward an impulse function, such turns will become sharp corners, and the the snakeboard will have to use the singular configuration to navigate them.

If we limit the torque applied at the rotor, then the rotor's maximum acceleration will be bounded by some $\ddot{\psi}_m$. From Eq. (16), the following inequality must be satisfied:

$$\frac{ML}{J_r}\left|\frac{2\dot{\xi}_x}{\sin 2\phi} + \dot{\phi}\sec^2\phi\xi_x\right| \leq \ddot{\psi}_m. \tag{25}$$

The first term on the left-hand side of Eq. (25) limits the forward acceleration of the snakeboard, especially when the wheel angles are near 0, $\frac{\pi}{2}$, and π. This is sensible, as we have seen that it becomes increasingly difficult for the snakeboard to control its forward velocity near these configurations.

The second term limits the forward velocity ξ_x itself. As $\phi \to \frac{\pi}{2}$, the snakeboard approaches its singular configuration, and the forward velocity ξ_x must decrease to prevent the term from becoming unbounded. In addition, the presence of $\dot{\phi}$ restricts the system from simultaneously traveling forward and changing directions too quickly.

In general, all of these joint limits prevent the snakeboard from turning arbitrarily quickly around a point of high curvature. The tighter the turn that the system has to make, the more it must slow down to do so without going off the prescribed path.

5 SIMULATIONS

We will now apply the general control solutions of Eq. (11) and Eq. (17) for the joint angles to some specific trajectory examples. In doing so, we will also refer to the special case results in Section 4.2 to analyze path feasibility and to characterize the system behavior.

As a motivating example, we will make use of track transition curves from civil engineering to construct trajectory profiles. Track transition curves smoothly connect straight and curved sections of roads and railway tracks [13, 14]. Such curves are usually formulated as higher-order polynomials that ensure that derivatives along the track remain continuous, thus minimizing changes in lateral acceleration to the locomoting system.

The path curvatures, as well as the desired velocities, that we command in the following examples consist mainly of straight sections connected by transition curve sections. We will prescribe the transition curvatures by the "fifth-order parabola" as shown in Table 3 of [14], which ensures smoothness of first derivatives. In addition, these polynomial curves can be integrated explicitly, so that we can obtain $r(t)$ if $\dot{r}(t)$ is described by a transition curve.

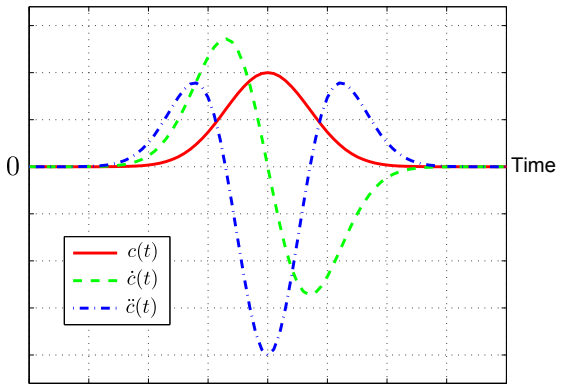

Figure 5. THE CURVATURE PROFILES OF A SHARP TURN.

Unless otherwise stated, we use the initial conditions $(x_0, y_0, \theta_0) = (0, 0, 0)$ for all simulations. We use the same snakeboard parameters as those in [9]:

$$M = 4, \quad J_r = 2, \quad J_w = \frac{1}{2}, \quad J = 1, \quad L = 1.$$

5.1 Constant Velocity Curves

We first consider the problem of maintaining constant velocity over turns with maximum curvature $c_0 = \kappa_0$. All turns start and end at arclengths of s_1 and s_2, respectively. The curvature κ is 0 for $s < s_1$ and $s > s_2$, and the two disjoint zero segments are smoothly connected by increasing and decreasing transition curves of varying magnitudes.

We simulate three trajectories with $c_0 = 0.1$, 0.2, and 0.3. For the distance function, we choose $r(t) = t$ such that the forward velocity is constant. Thus, the rotor profile is easily determined by (18), while the wheel angle comes from Eq. (11).

The snakeboard's resultant trajectories, along with snapshots at equal time intervals, is shown in Fig. 6. The system follows all curves with constant velocity, as expected. Note that the larger the maximum curvature, the greater the turn achieved.

5.2 Accelerating Over Nonzero Curvature

We have seen that the snakeboard cannot change its forward velocity while traveling straight. One way that the system can circumvent this is to temporarily deviate from its path on a curved segment, accelerate, and then resume its original path.

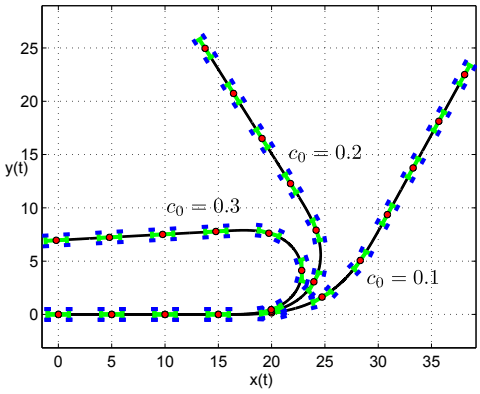

Figure 6. CONSTANT VELOCITY TRAJECTORIES.

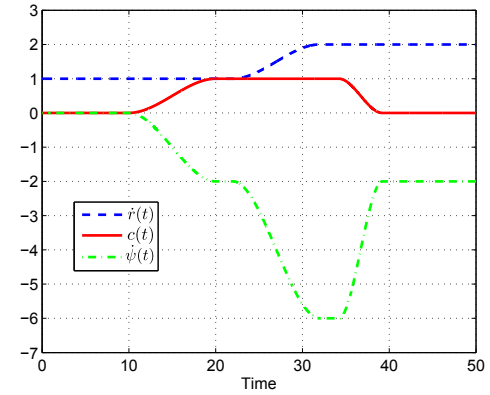

Figure 7. TRAJECTORY AND ROTOR INPUT PROFILES.

Here we will accelerate on a constant curvature only, using the analytical result of Eq. (21).

As shown in Fig. 7, the curvature $c(t)$ has three segments of constant curvature connected by two transition curves. The desired velocity $\dot{r}(t)$ is constant nearly everywhere, and its transition curve occurs in the regime where c is constant and nonzero. From these functions we can find $\dot{\psi}(t)$, using both Eq. (18) and Eq. (21).

Figure 8 shows the trajectory of the snakeboard, which executes the maneuver described by doubling its velocity after the curved section. We also superimpose the rotor velocity $\dot{\psi}(t)$ on top of the trajectory profiles in Fig. 7. Note how the rotor must accelerate to either maintain the system's constant forward velocity while path curvature is changing, or to change forward velocity on a constant curvature path.

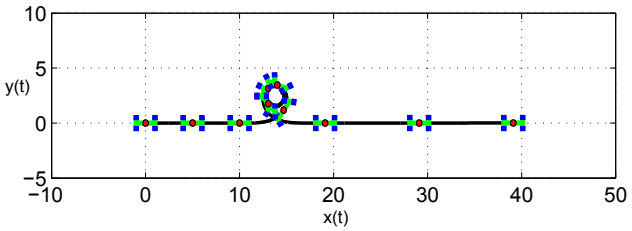

Figure 8. ACCELERATING ON CONSTANT CURVATURE.

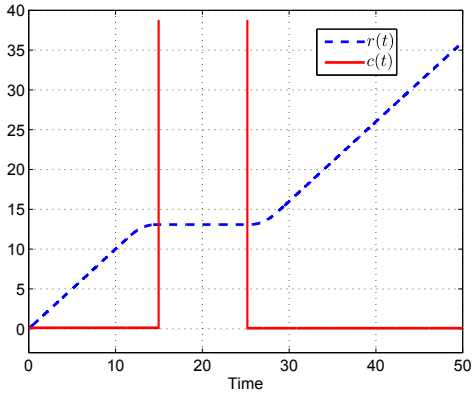

Figure 9. TRAJECTORY PROFILE WITH A CORNER.

5.3 A Trajectory with Corners

For the last example, we demonstrate an example trajectory with a sharp corner. We have shown that one way of maneuvering a corner is equivalent to stopping, reorienting the system, and then moving again. Figure 9 shows both the curvature $c(t)$ and desired distance function $r(t)$.

The period during which $c(t)$ is infinite and $r(t)$ is constant exactly corresponds to when the snakeboard is at the corner. The traveled distance r should not change while the snakeboard is not moving forward, while c is described by an impulse function.

Figure 10 shows the wheel angles and orientation of the snakeboard. Note the ordering of the steps in the turning maneuver: ϕ first goes to $\frac{\pi}{2}$, and then θ aligns with the new path by rotation action of the rotor. When that is complete, ϕ turns to its new angle, and then the system again resumes its locomotion.

6 CONCLUSIONS

We have presented explicit solutions for the inverse motion planning problem for the snakeboard. In doing so, we rely only on local trajectory information of curvature and arclength, and the solution is simple and easy to analyze due to our choice of body coordinates. We take advantage of their forms to derive

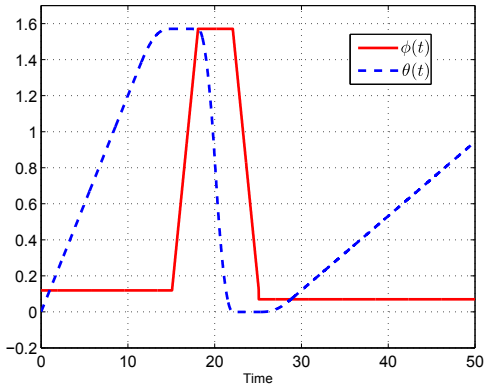

Figure 10. WHEELS AND ROTOR DURING A CORNER MANEUVER.

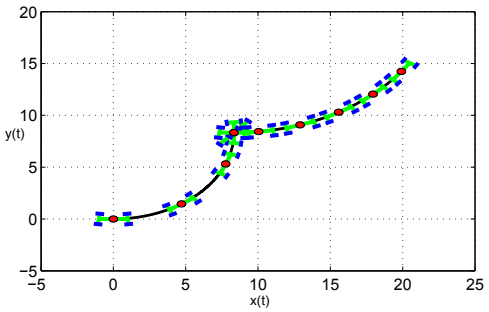

Figure 11. MANEUVERING A CORNER.

motion primitives, as well as a method for dealing with non-differentiable paths. Finally, we discussed practical limitations that may be taken into account for a real system.

Since we now know what types of trajectories the snakeboard can and cannot follow, future work may revisit the problem in which only the initial and goal states are provided. These results can be combined with the latest work in path planning in order to construct efficient paths that are easy to follow, especially paths that consist mainly of constant curvature sections.

Another interesting direction would be to investigate how much the usage of body coordinates generalizes in simplifying solutions for dynamical systems. While they can present simpler solutions than their inertial coordinate counterparts, using them to move back into the world frame to compute various quantities can often be a difficult or computationally expensive problem.

REFERENCES

[1] Ostrowski, J., Burdick, J., Lewis, A., and Murray, R., 1995. "The mechanics of undulatory locomotion: the mixed kinematic and dynamic case". In Robotics and Automation, 1995. Proceedings., 1995 IEEE International Conference on, Vol. 2, pp. 1945 –1951 vol.2.

[2] Shammas, E. A., Choset, H., and Rizzi, A. A., 2007. "Towards a unified approach to motion planning for dynamic underactuated mechanical systems with non-holonomic constraints". *The International Journal of Robotics Research,* **26**(10), pp. 1075–1124.

[3] Ostrowski, J., Lewis, A., Murray, R., and Burdick, J., 1994. "Nonholonomic mechanics and locomotion: the snakeboard example". In Robotics and Automation, 1994. Proceedings., 1994 IEEE International Conference on, pp. 2391–2397 vol.3.

[4] Murray, R., and Sastry, S. S., 1993. "Nonholonomic motion planning: Steering using sinusoids". *IEEE Transactions on Automatic Control,* **38**, pp. 700–716.

[5] Ostrowski, J., Desai, J., and Kumar, V., 1997. "Optimal gait selection for nonholonomic locomotion systems". In Robotics and Automation, 1997. Proceedings., 1997 IEEE International Conference on, Vol. 1, pp. 786–791 vol.1.

[6] Bullo, F., and Lewis, A., 2003. "Kinematic controllability and motion planning for the snakeboard". *Robotics and Automation, IEEE Transactions on,* **19**(3), June, pp. 494–498.

[7] Bullo, F., Member, A., and Lynch, K. M., 2001. "Kinematic controllability for decoupled trajectory planning in underactuated mechanical systems". *IEEE Transactions on Robotics and Automation,* **17**, pp. 402–412.

[8] Shammas, E., and de Oliveira, M., 2011. "An analytic motion planning solution for the snakeboard". In Proceedings of Robotics: Science and Systems.

[9] Shammas, E., and de Oliveira, M., 2012. "Motion planning for the snakeboard". *The International Journal of Robotics Research,* **31**(7), pp. 872–885.

[10] Kelly, S. D., and Murray, R. M., 1995. "Geometric phases and robotic locomotion". *Journal of Robotic Systems,* **12**(6), pp. 417–431.

[11] Ostrowski, J., and Burdick, J., 1996. "The geometric mechanics of undulatory robotic locomotion". *INTERNATIONAL JOURNAL OF ROBOTICS RESEARCH,* **17**, pp. 683–701.

[12] Bloch, A. M., Krishnaprasad, P. S., Marsden, J. E., and Murray, R. M., 1996. "Nonholonomic mechanical systems with symmetry". *ARCH. RATIONAL MECH. ANAL,* **136**, pp. 21–99.

[13] Lipicnik, M., 1998. "New form of road/railway transition curve". *Journal of transportation engineering,* **124**(6), pp. 546–556.

[14] Long, X., Wei, Q., and Zheng, F., 2010. "Dynamic analysis of railway transition curves". *Proceedings of the Institution of Mechanical Engineers, Part F: Journal of Rail and Rapid Transit,* **224**(1), pp. 1–14.